Journal of Geophysical Research: Atmospheres

RESEARCH ARTICLE
10.1029/2018JD028911

Comparison of Daytime Low-Level Cloud Properties Derived From GOES and ARM SGP Measurements

Theodore M. McHardy[1], Xiquan Dong[1], Baike Xi[1], Mandana M. Thieman[2], Patrick Minnis[3], and Rabindra Palikonda[2]

[1]Department of Hydrology and Atmospheric Sciences, University of Arizona, Tucson, AZ, USA, [2]SSAI, Inc., Hampton, VA, USA, [3]NASA Langley Research Center, Hampton, Hampton, VA, USA

Key Points:
- Passive satellite-retrieved cloud effective temperature has a cold bias compared to surface-based cloud top temperature
- Effective radius is overestimated by the satellites; a large portion of this bias occurs when the scattering angle is low
- Overall, cloud temperature, optical depth, and liquid water path are fairly well correlated with surface-based retrievals

Supporting Information:
- Supporting Information S1
- Table S1
- Table S2
- Table S3

Correspondence to:
X. Dong,
xdong@email.arizona.edu

Citation:
McHardy, T. M., Dong, X., Xi, B., Thieman, M. M., Minnis, P., & Palikonda, R. (2018). Comparison of daytime low-level cloud properties derived from GOES and ARM SGP measurements. *Journal of Geophysical Research: Atmospheres*, *123*, 8221–8237. https://doi.org/10.1029/2018JD028911

Received 22 SEP 2017
Accepted 6 JUL 2018
Accepted article online 20 JUL 2018
Published online 13 AUG 2018

Abstract Large-scale satellite data are critical for both verifying and improving general circulation model parameterizations of clouds and radiation for climate prediction. For reliable application of satellite data sets in cloud processes and climate models, it is important to have a reasonable estimate of the errors in the derived cloud properties. The daytime single-layered low-level cloud properties retrieved by the Geostationary Operational Environmental Satellite system (GOES) are compared with ground-based observations and retrievals over the Department of Energy Atmospheric Radiation Measurement (ARM) Southern Great Plains (SGP) Central Facility from June 1998 to December 2006. The GOES retrievals are made via the Visible-Infrared Solar-infrared Split-window Technique. They are spatially averaged within a $0.15° \times 0.15°$ box centered on the ARM SGP site, and the ARM surface observations are temporally averaged ±15 min around the GOES scans to produce collocated pairs. Comparisons are made for monthly means, diurnal means, and one-to-one GOES and ARM collocated pairs. GOES T_{eff} is highly correlated with ARM T_{top} cloud temperature, having an R^2 value of 0.75, though GOES exhibits a cold bias. GOES-retrieved τ and liquid water path have very good agreement with ARM retrievals with R^2s of 0.45 and 0.47, while r_e (GOES), on average, is about 2 μm greater than ARM r_e. An examination of solar and viewing geometry has shown that GOES-retrieved mean r_e and τ values are impacted by solar zenith angle and especially scattering angle, which is not unexpected and needs to be accounted for by users.

1. Introduction

Clouds are well established as a major source of uncertainty in climate prediction (Intergovernmental Panel on Climate Change, 2014; Wielicki et al., 1995) and modeling (Randall et al., 2003). They are also the dominant modulators of radiation both at the surface and at the top of the atmosphere, and their impact on the Earth's radiation budget mainly depends on their bulk properties such as cloud amount, height, and microphysical/optical characteristics (Curry et al., 2000; Houghton et al., 2001). Characterizing cloud radiative effects at the surface and at the top of the atmosphere is critical in understanding the current climate and an important step toward simulating potential climate change. Large-scale satellite data are needed to both verify and improve general circulation model parameterizations of clouds and radiation for climate prediction. For reliable application of satellite data sets in cloud processes and climate models, it is important to have a reasonable estimate of the bias and uncertainty in the derived cloud properties. Ideally, this should be done via in situ aircraft measurements (e.g., Dong et al., 1998, 2002; Dong & Mace, 2003; Min et al., 2003; Painemal et al., 2012). However, flight hours are expensive and limited; thus, satellite retrievals are often validated with long-term ground-based instruments (e.g., Dong et al., 1998, 2016; Min et al., 2004; Smith et al., 2008; Xi et al., 2010, 2014; Yan et al., 2015; Zhang et al., 2017). Comparisons between the ground- and satellite-based observations must be conducted carefully because of significant spatial and temporal differences between the two observing platforms. Also, because clouds are so variable, a statistically reliable comparison requires many cloud events observed by both satellite and surface.

The Geostationary Operational Environmental Satellite system (GOES) provides the unique combination of large areal coverage and relatively high spatial and temporal resolutions and has been used to provide cloud property retrievals for over three decades (e.g., Minnis et al., 1995; Minnis & Harrison, 1984; Minnis & Smith, 1998; Rossow & Schiffer, 1991). Even for data used as extensively as those from GOES, it is important to continuously work at evaluation as new product versions and techniques are implemented. Studies during the past decade have focused on validating GOES cloud property retrievals for tropical high

clouds during the Tropical Composition, Cloud and Climate Coupling (TC4) field campaign (Chang et al., 2010; Yost et al., 2010) and warm marine boundary layer clouds during the Variability of the American Monsoon Systems (VAMOS) Ocean-Cloud-Atmosphere-Land Study Regional Experiment (VOCALS-REX) campaign (Painemal et al., 2012; Wood et al., 2011). Because of their large areal coverage, marine stratocumulus clouds have been examined extensively (Dong, Xi, Kennedy, et al., 2014; Dong, Xi, & Wu, 2014; Wood et al., 2015; Wu et al., 2015, 2017), and satellite cloud retrievals have been validated using ARM Azores observations (Xi et al., 2014). In comparison, stratocumulus clouds over land cover 12% of the surface, on average (Wood, 2012), but are relatively understudied (Dong et al., 2005; Kollias et al., 2007).

Low-level stratus cloud microphysical properties derived from surface-based and GOES data during the March 2000 cloud intensive observational period at the Atmospheric Radiation Measurement (ARM) program Southern Great Plains (SGP) site were compared with aircraft in situ measurements (Dong et al., 2002). During the intensive observational period, four low-level stratus cases were observed by the ground- and satellite-based remote sensors and aircraft in situ instruments resulting in a total of 10 hr of simultaneous data from the three platforms. Both ground- and satellite-based retrieved cloud microphysical properties agree with aircraft in situ measurements within 10% except for GOES-retrieved cloud droplet effective radius r_e, which averaged 23% or 1.8 μm greater than the aircraft results. Xi et al. (2010) analyzed one decade of ARM radar-lidar and GOES observations at the ARM SGP Central Facility (36.60°N, 97.49°W) and concluded that there is excellent agreement in the long-term mean cloud fractions. The long-term statistics of low-level stratus cloud microphysical properties over the SGP have been investigated by a quite few studies (e.g., Chiu et al., 2010; Dong et al., 2005; Sengupta et al., 2004); however, there is not yet a statistical comparison in low-level stratus cloud microphysical properties between ARM and GOES.

The ARM SGP Central Facility was established by the Department of Energy (DOE) in 1993 (Ackerman & Stokes, 2003; Mather & Voyles, 2013; Sisterson et al., 2016; Stokes & Schwartz, 1994) to improve the understanding of clouds and radiation and developing model parameterizations using surface observations over climate temporal scales. With an expansive suite of instruments, this site provides one of the best facilities in the world for satellite-based cloud property retrieval validation. This study is primarily an evaluation of GOES-retrieved terrestrial stratocumulus microphysical and macrophysical properties using cloud microphysical property retrievals at the ARM SGP from June 1998 to December 2006. The purpose is to characterize and improve the use of these GOES data. Comparisons are made based on monthly means, diurnal (hourly) means, and one-to-one for spatiotemporally collocated pairs in order to provide long- and short-term context. Section 2 of this paper contains information on the GOES and ARM data sets used in this study and collocation and filtering. Section 3 provides the results of various comparisons made between the GOES and ARM cloud property retrievals on multiple temporal scales. Section 4 concludes and summarizes the salient findings of this study.

2. Data and Methodology

2.1. GOES Data

The GOES cloud products used in this study were retrieved using algorithms originally developed for the NASA Clouds and Radiant Energy Systems (CERES) project (Minnis et al., 2011, 2008) and adapted for application to other imagers on geostationary (Minnis et al., 2008) and low Earth-orbit satellites under the umbrella of the Satellite Cloud and Radiation Property retrieval System (SatCORPS; Minnis et al., 2016). Retrievals from GOES are used for CERES time and space averaging and have been provided in support of the ARM program for over two decades (e.g., Ayers et al., 2006). The retrievals in this study are available every 30 min (at 15 and 45 min past the hour) at a 4-km horizontal resolution and were produced using the ARM SatCORPS Versions 2.1 and 3.0 for GOES-8, GOES-10, and GOES-11. Table 1 lists details concerning the satellites, data versions, and time periods. The results were taken from the ARM Climate Research Facility Data Archive (https://archive.arm.gov).

GOES-8, GOES-10, and GOES-11 were launched on 13 April 1994, 25 April 1997, and 3 May 2000, respectively. The former was located at 75°W, while the latter two were at 135°W. The GOES visible channels were calibrated against the Collection 5 Aqua Moderate-resolution Imaging Spectroradiometer (MODIS) 0.64-μm channel as in Minnis et al. (2002). For GOES satellites, the visible channel radiance is

Table 1
The Satellite, Position, Time Period, and SatCORPS Version for the GOES Data Used in This Study

Satellite	Position	Period	Version	g_0	g_1	g_2	C_0
GOES-8	East	5/1/1998–12/31/1998	2.1	0.6497	1.34E−04	0	31
		1/1/1999–12/31/1999	2.1	0.562	2.22E−04	−2.43E−08	29
		1/1/2000–3/30/2003	3	0.562	2.22E−04	−2.43E−08	29
GOES-10	West	4/1/2003–8/31/2005	3	0.478	2.22E−04	−3.13E−08	29
		9/1/2005–6/20/2006	2.1	0.478	2.22E−04	−3.13E−08	29
GOES-11	West	6/21/2006–12/31/2006	3	0.518	7.32E−05	0	29

Note. GOES East is at 75°W and GOES West is at 135°W. Here C_0 is the visible channel offset, and g_0, g_1, and g_2 are calibration coefficients.

$$L = \left(g_0 + g_1 d + g_2 d^2\right)(C - C_0), \tag{1}$$

where L is the visible radiance (0.65 μm), d is number of days since launch, C is the 10-bit brightness count, C_0 is the visible channel offset, and g_0, g_1, and g_2 are calibration coefficients (Nguyen et al., 2004). The values of the parameters for each satellite and time period can be found in Table 1 and are included in the data files available on the ARM data archive. Reflectance for each satellite was computed as the ratio of the radiance to the Earth-Sun and solar zenith angle-corrected solar constant. A common value of 526.9 $W \cdot m^2 \cdot sr$ was used for the solar constant.

Pixels are first classified as cloudy or clear, and retrievals are performed using cloudy pixel radiances. Cloudy pixel identification techniques are different for daytime (solar zenith angle, SZA $<$ 82°), twilight (82° $\leq$ SZA $\leq$ 88.5°), and nighttime (SZA $>$ 88.5°), and for polar (Trepte et al., 2002) and nonpolar (Minnis et al., 2008) regions, resulting in six cloud masks. The cloud effective radiating temperature (T_{eff}) is retrieved by correcting the observed radiance at 10.8 μm for atmospheric and surface emission and absorption. It is the radiating temperature at the level corresponding to an optical depth (τ) of 1.0–1.5 below the cloud physical top for clouds having $\tau > 5$ (Minnis et al., 2008). The level rises and the corresponding τ decreases as the viewing zenith angle increases. For low-level water clouds, this level typically corresponds to an altitude ~100 m below the cloud top (Dong et al., 2008), depending on the τ and viewing geometry. Although cloud height retrievals from GOES are used here as a data filter (section 2.3), they are not examined in this study as the retrieval algorithm for low clouds used in the currently available product is outdated and has been revised in newer versions (Sun-Mack et al., 2014). The cloud effective height (H_{eff}) is estimated by matching T_{eff} to a vertical temperature profile. For ARM SatCORPS Versions 2.1 and 3.0, Rapid Update Cycle (RUC; Benjamin et al., 2004) temperature profiles are used for pressure, $p \leq 500$ hPa. For the boundary layer ($p > 700$ hPa), a lapse rate (Γ) of −7.1 K/km anchored to the RUC surface temperature is used for the temperature profile (Minnis et al., 1992, 2003, 2011). For 500 hPa $< p \leq 700$ hPa, Γ is adjusted linearly such that the resulting temperature at 500 hPa matches that of the RUC profile. Smith et al. (2008) show that while this algorithm produces cloud heights that are well correlated with ground-based observed cloud heights overall, it appears to perform worse for low clouds.

This study is daytime only because the passive satellite retrievals of cloud microphysical properties are more robust when visible channels are available. The GOES cloud microphysical properties are retrieved based on the Visible-Infrared Solar-infrared Split-window Technique, which is a version of bispectral method that uses an iterative look-up table approach (Minnis et al., 2011). Look-up tables are constructed for water droplet and ice crystal clouds based on viewing geometry and atmospheric and surface corrections for a range of τs from 0.25 to 128 and a range of cloud droplet effective radii (r_e) from 2 to 32 μm (Minnis et al., 1998). The τ and r_e retrievals primarily utilize the visible channel and 3.9-μm band, respectively. The cloud liquid water path (LWP) is computed from the retrieved τ and r_e values ($\frac{2}{3} * \rho_l * \tau * r_e$, where ρ_l is the density of water). This equation assumes that the clouds are vertically homogenous, although studies have shown an overestimation of LWP due to the retrieved r_e in upper portion of boundary layer clouds (Dong et al., 2008; Miller et al., 2016; Xi et al., 2014). A discussion on uncertainty in the microphysical property retrieval algorithm can be found in Dong et al. (2008), though it is written regarding the CERES-MODIS version of the algorithm.

Table 2
A List of Cloud Properties Obtained From the ARM SGP Site, Their Approximate Uncertainty, and Sources for Any Algorithms Used in Their Retrievals

Cloud property	Full name	Uncertainty	Instrument and retrieval algorithm
ARM T_{base} and T_{top}	Cloud base and top temperature (K)	0.2 °C	Merged Sounding (Troyan, 2012)
ARM r_e	Cloud droplet effective radius (μm)	~10% for daytime	Dong et al. (1997, 1998, 2002)
ARM τ	Cloud optical depth	~5–10% for daytime	Dong et al. (1997, 1998, 2002)
ARM LWP	Cloud liquid water path (g/m^2)	~10%	Microwave radiometer (Liljegren et al., 2001)

2.2. ARM Surface Data

Table 2 lists the cloud properties from the ARM SGP site utilized in this study, the instruments used to retrieve them, their approximate uncertainties, and sources. These data were obtained as 5-min averages; additional processing will be discussed in section 2.3. Cloud base height (H_{base}) and cloud top height (H_{top}) are from the Active Remote Sensing of Clouds (Clothiaux et al., 2001) product, which incorporates three ground-based active remote sensing instruments. This product has vertical and temporal resolutions of 45 m and 10 s, respectively. Also provided are cloud classifications, which delineate clouds based on height (low, middle, and high) for multiple layers based on reflectivities from the Millimeter wavelength Cloud Radar (MMCR; Moran et al., 1998). Clouds within an inversion layer, labeled as "overturning" clouds, are also identified. Having a wavelength of 8 mm, the MMCR is able to penetrate multiple cloud layers and is used to derive H_{top}. Because the MMCR can be sensitive to drizzle or ground clutter, such as insects below the cloud base (but not necessarily above it; Dong et al., 2008), a ceilometer and micropulse lidar are also used in the retrieval of H_{base}. Further details on the cloud height retrieval algorithms can be found in Clothiaux et al. (2000). The cloud base and cloud top temperatures (T_{base} and T_{top}) are retrieved by matching the H_{base} and H_{top} to the Merged Sounding Value-Added Product (Troyan, 2012), which is available at 1-min temporal and 20 m (below 3 km above ground level; 50 m above 3 km) vertical resolution.

The LWP is derived based on brightness temperatures at 23.8 and 31.4 GHz, which are measured with a microwave radiometer (Liljegren et al., 2001). Daytime microphysical properties are retrieved based on the method described in Dong et al. (1997), which utilizes a δ2-stream radiative transfer model and ground-based measurements. Dong et al. (1998) parameterized this method to retrieve r_e based on LWP, solar transmission, and the cosine of the SZA. Once cloud r_e is obtained, it is used in conjunction with the microwave radiometer retrieved LWP to compute τ (Min & Harrison, 1996). It is important to note that for ARM surface data, LWP and r_e are retrieved and then used to compute τ, while for GOES, τ and r_e are retrieved and then used to compute LWP. The Dong et al. (1998) parameterization is only performed when these five criteria, which are discussed in detail by Dong et al. (2000), are met: (1) Cloud radar determines only single-layered overcast clouds that are present, (2) H_{top} is lower than 4 km, (3) 20 g/m^2 < LWP < 700 g/m^2, (4) cos(SZA) > 0.2 (which corresponds to a SZA of <78.5°), and (5) solar transmission is between 0.1 and 0.7. GOES- and ARM-retrieved τ and r_e are only compared when the ARM retrievals are available, while LWP, and temperature are compared whenever those values are available.

2.3. Collocation and Filtering

A direct comparison between GOES- and ARM-retrieved cloud properties is desired, therefore the results from the two different platforms must be temporally collocated. Additional averaging is required because the data retrieved at the ARM SGP site essentially represent conditions continuously at a point, while GOES pixels cover an area of approximately 4 km × 4 km at a specific point in time. The surface data are averaged every 5 min, while GOES images are half-hourly snapshots. Dong et al. (2002, 2008) demonstrated that temporally averaging ARM surface data and spatially averaging GOES data to account for cloud movement over the ARM site produces robust comparisons. The methodology used in collocating these two data sets is as follows. GOES cloud properties are averaged within a 0.15° × 0.15° box centered over the ARM SGP site. Then, ARM surface data taken within ±15 min (six data points, avoiding duplicate use of the ARM data) of each GOES image are averaged, and the ARM-GOES pairs are made.

Daytime, single-layered, overcast, low-level water clouds are the focus of this study; therefore, the collocated data must be filtered to remove results from clear skies and other cloud types. Because the Dong et al. (1998) cloud microphysical property retrieval parameterization is only available during the daytime, twilight and

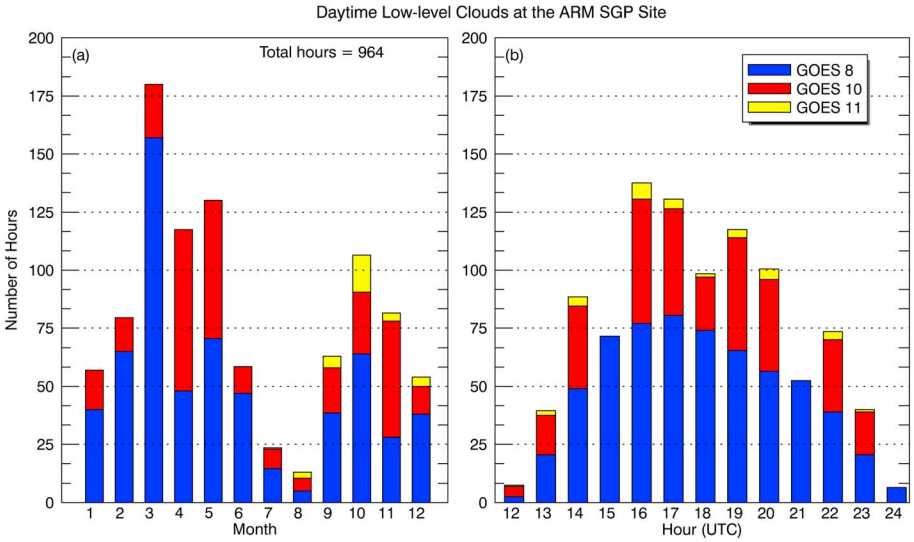

Figure 1. (a) The number of hours of daytime (solar zenith angle <82°) single-layered low-level clouds over the ARM Southern Great Plains (SGP) site from May 1998 to 2006, binned by month and colored by GOES satellite. Due to temporal averaging, each hour represents two half-hour data points in this study. Note that July and August have low data counts, which limits the robustness of conclusions drawn about daytime low cloud properties during these two months. (b) Same as Figure 1a except that the data are binned by UTC time (local noon ~18 UTC). The time indicated by the *x* axis is the bin start time.

nighttime data are removed by limiting the SZA to 82°. Next, all data points not identified by the MMCR as single-layered low clouds, low with multiple layers, or overturning clouds are removed in this study. Then, data with an ARM-retrieved T_{base} less than 250 K or a mean (for the 0.15° × 0.15° box) GOES *He*ff greater than 4 km are also removed in order to limit high cloud contamination from either source. The cloud fraction within the GOES average box must be 1.0; that is, all GOES pixels within the 0.15° × 0.15° box centered on the ARM SGP site must be identified as cloudy. Finally, any times with a surface MWR-retrieved LWP greater than 500 g/m^2 are excluded in order to limit cases coinciding with the occurrence of precipitation. Saavedra et al. (2012) show that nonprecipitating clouds can have LWP values up to 550 g/m^2. However, Löhnert and Crewell (2003) suggest that cloud LWP retrievals deteriorate approaching 700 g/m^2. Although precipitation can occur in marine stratus clouds with LWP below 200 g/m^2 (Saavedra et al., 2012), only 20% of the data used in this study have surface-retrieved LWP greater than that (Figure 6) and less than 10% of the data have LWP greater than 300 g/m^2. Because this study is terrestrial, it is even more unlikely that the results from this study are impacted by the occurrence of precipitation. Following these filters, outliers were identified by cloud optical depth (based on Figure 6b). MMCR vertical profiles, GOES imagery, and snow cover maps were visually inspected, and data taken when high clouds or snow cover were present were removed (~60 data points). The remaining data points are used in the analysis presented below.

3. Results and Discussions

The temporal variation of daytime low-level liquid clouds over the ARM SGP site is examined in two ways. First, Figure 1a shows the number of hours of data binned by month from June 1998 to December 2006 and colored by the GOES satellite used. Note that 1 hr of data is equivalent to two pairs of collocated data points, because GOES data are available every half hour. In other words, the total number of hours of data is equal to the number of data points divided by 2. Low-level liquid clouds occur most frequently during spring (March-April-May), moderately frequently in fall (September-October-November) and winter (December-January-February), and least frequently during summer (June-July-August). The total number of hours of data is 964 (1,928 data points). For context, Xi et al. (2010) found that low-level clouds (defined as having a cloud top height < 3 km) with no other clouds above occur roughly 10% of the time over SGP. This distribution is similar to the results in Kennedy et al. (2013). It is important to point out that the amount of data for July and August is low (<20 hr), so the results presented for these two months should be interpreted with caution.

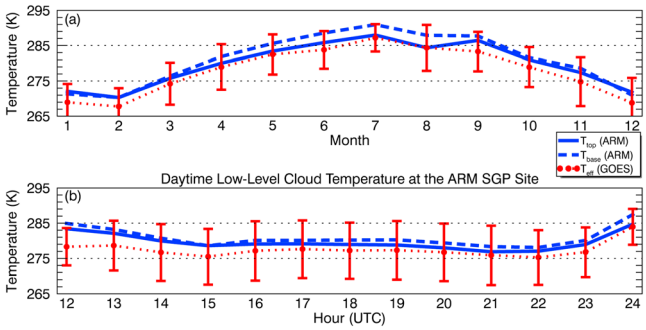

Figure 2. (a) Monthly mean cloud top (T_{top}, blue solid line) and base (T_{base}, blue dashed line) temperatures from ARM observations and cloud effective temperature (T_{eff}, red circles) retrieved from GOES observations over the ARM SGP site. The monthly standard deviations of GOES effective temperature are indicated by the error bars. (b) Same as (a) except for hourly means.

Next, the diurnal cycle (daytime only) is shown in Figure 1b with UTC time. Note that local noon at the ARM SGP is ~18 UTC. The labels indicate the time at the start of the bin; that is, the first bin includes data points occurring between 12 and 13 UTC. The cloud samples have a roughly normal distribution with the maximum occurring around local noon (16–20 UTC) and minimum occurring at sunrise (12 UTC) and before sunset (24 UTC). The minimum frequency occurrences during early morning and late evening are likely due to the SZA filter (SZA $< 82°$) in this study. This is because days that meet this solar geometry criterion before 13 UTC and after 24 UTC only occur during a limited part of the summer season. Thus, the results at 12 and 24 UTC should be used with caution. At the winter solstice, a SZA of 82° occurs just before 15:00 and after 22:00 UTC. Therefore, bins containing hours from 15 to 22 UTC are unaffected by the solar zenith angle filter. In other words, the decline in low-level cloud frequency seen from 15 UTC through the rest of the day is genuine and not due to sampling bias.

3.1. Cloud Temperature

To compare GOES and ARM retrievals, monthly mean cloud temperatures (top and base from ARM, effective from GOES), based on all matched samples shown in Figure 1, were computed and are presented in Figure 2a. The seasonal and monthly mean values of cloud temperature and microphysical properties are provided in the supporting information reference. The means and standard deviations for the seasonal and monthly differences between the ARM and GOES values are also reported. Note that these means were computed using all points having valid data for GOES and ARM individually, while means and standard deviations shown on scatter-density plots (e.g., Figure 3) are computed using all collocated GOES and ARM results. For clarity, T_{eff} will always refer to GOES-retrieved cloud effective temperature and T_{base}/T_{top} will refer to the ARM retrievals in the following discussion, unless specifically stated as otherwise. The monthly mean cloud temperature follows an intuitive pattern, with the highest average temperature (~290 K) occurring in July and the lowest mean temperature (~270 K) occurring in February. The differences between T_{base} and T_{top} increase from −0.5 K in winter to +2.9 K in summer and then decrease toward the winter months, indicating that there are thicker clouds and/or greater lapse rates within the clouds during late spring and summer months. The monthly mean T_{eff} generally follows the seasonal variations of the T_{base} and T_{top} but are ~3 K colder than both T_{base} and T_{top} throughout the course of a year. Nevertheless, all monthly mean T_{base} and T_{top} values fall within one standard deviation of the T_{eff}.

In addition to the monthly mean comparisons, the hourly mean cloud temperatures derived from both ARM and GOES observations are presented in Figure 2b. The T_{base} and T_{top} means are at a maximum (~287 K) in the morning and decrease throughout the day until the midafternoon hours (275 K at 21 UTC), after which they begin increasing again. T_{eff} values follow the same pattern, though less noticeably. This variation is partially due to a sampling bias; that is, the earliest and latest UTC hours only contain data from summer months due to the SZA filter; however, data taken between 15 and 22 UTC include all months and have no sampling bias. On average, there is a small decrease of cloud temperature with local time for those hours. The T_{top} (ARM) − T_{eff} (GOES) mean temperature difference is greatest early in the morning and relatively constant between 15 and 22 UTC. This behavior may, in part, be the result of underestimating cloud optical depth in the limited summer sampling (see next section). Minnis et al. (2011) discusses the *T*eff retrieval in detail and how τ can affect it.

To compare GOES and ARM retrievals directly, scatter-density plots of T_{top} versus collocated T_{eff} are plotted and shown in Figure 3. Also shown on the plots are the total number of data pairs (N), the coefficient of determination (R^2), and the means and standard deviations of GOES and ARM retrievals (mean/standard deviation). As demonstrated in Figure 3a, although their mean difference is 2.0 K, most of collocated T_{eff} and T_{top} values are located just below the 1:1 line with an R^2 value of 0.75. The consistent cold bias of T_{eff} versus the T_{base} and T_{top} values seen in Figure 2 is also evident in Figure 3a. Figure 3b shows the probability density functions (PDFs) and cumulative distribution functions (CDFs) for T_{top} and T_{eff}. The T_{eff} values are fairly evenly distributed, which can be seen in the lack of peak in the PDF and the quasi-linear CDF. The distribution of T_{top}

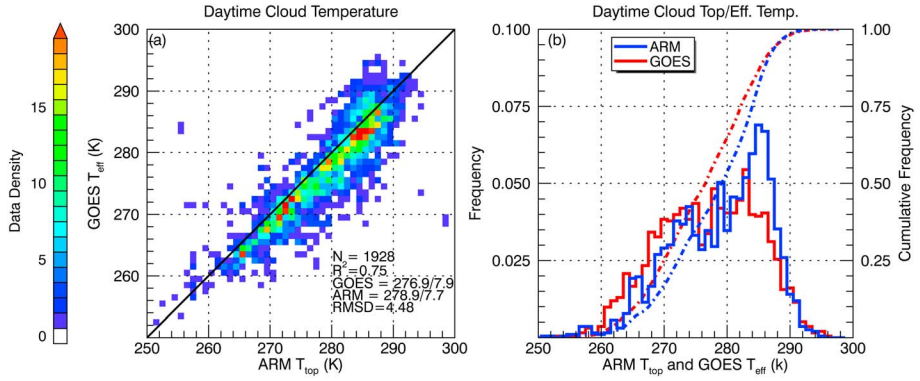

Figure 3. (a) Scatter-density plots of cloud top temperature (T_{top}) from ARM versus GOES cloud effective temperature (T_{eff}). Each data point represents the GOES and ARM values of a spatiotemporally collocated pair. Data point density values are indicated by the color bar on the left. The one-to-one line is shown. The total number of data points (N), coefficient of determination (R^2), and mean and standard deviation (mean/standard deviation) for GOES and ARM data are presented in each plot. (b) Probability density functions (PDFs, solid lines) and cumulative distribution functions (CDFs, dotted lines) for T_{eff} (red) and T_{top} (blue). The bin size for both figures is 1 K.

is negatively skewed (to the left), due to the substantial peak in frequency at higher values. The consistent cold bias of T_{eff} with respect to T_{top} can again be seen in the CDFs.

Because this study utilizes GOES T_{eff} instead of GOES T_{top}, a warm bias would be expected given a monotonically decreasing temperature profile and the nature of T_{eff} and T_{top}. The cold bias found here is consistent with, but greater in magnitude than seen in previous comparisons of satellite T_{eff} with T_{top} from in situ (Painemal & Zuidema, 2011), and surface radar/rawinsonde (Xi et al., 2014) over ocean, which showed values ranging from −0.9 K during daytime to −2.0 K at night. Similar magnitudes were observed by Dong et al. (2008) in their comparison of MODIS and ARM SGP retrievals that varied from −1.1 K in early afternoon to −2.9 K after midnight. The results in Figure 3a also indicate that the magnitude of the differences between T_{eff} and T_{top} bottoms out during the early afternoon and tends to increase toward sunset. To be sure that this is not due to the merged sounding products interpolation, GOES T_{eff} − ARM T_{top} was plotted as a function of the time from the closest actual balloon launch (not shown). There was no significant relationship between the time distance and the magnitude of the bias or error. Painemal et al. (2013) compared GOES T_{top} with aircraft in situ data for marine boundary layer clouds and found a similar cold bias and discuss this cold bias in some detail regarding the sign and magnitude of possible sources. They hypothesized that the $T_{eff} - T_{top}$ difference could be due to evaporative and/or longwave cooling of droplets at the cloud top. These processes would tend to cool the cloud droplets, which are the primary emission source contributing to T_{eff}. Because longwave cooling and entrainment should be the greatest at night and the early morning (Bretherton et al., 2010; Caldwell & Bretherton, 2009), they could be the main driving force of the negative temperature differences. Figure 2 shows that $T_{eff} - T_{top}$ does indeed peak in the early morning and decrease throughout the day, suggesting that longwave cooling of the cloud droplets may be the dominant process here. Yet several studies have demonstrated that the surface of an evaporating droplet can be significantly cooler than the surrounding air and the temperature difference depends on the evaporation rate (e.g., Johnson, 1950; McGaughey & Ward, 2002). Evaporation rates are inversely proportional to the relative humidity of the ambient air and, hence, to the entrainment rate of dry air. As inversions at the cloud top deepen, they increase the entrainment rate. This deepening typically occurs at night as the result of the longwave cooling. Thus, the longwave cooling could impact T_{eff} in two ways: directly through radiative loss and indirectly through increased evaporation due to the resulting increase in entrainment. As this cold bias is found in multiple studies, which utilize both surface-based and aircraft data, it is unlikely that is due solely to instrumentation/retrieval error. Additional insight into this phenomenon would require some detailed microphysical process modeling and analysis, which are beyond the scope of this study.

3.2. Cloud Microphysical Properties

Cloud microphysical properties are examined in the same way as cloud temperature. Figure 4 shows the monthly means of cloud droplet effective radius (r_e), cloud optical depth (τ), and liquid water path (LWP)

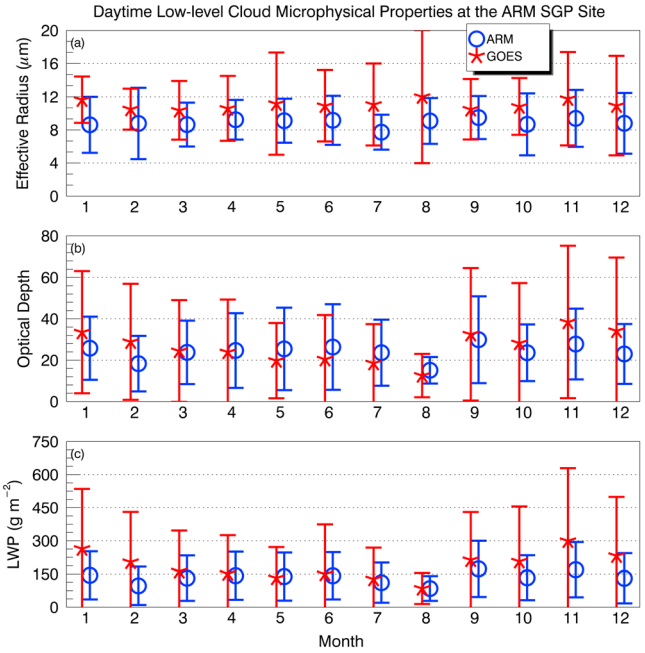

Figure 4. Same as Figure 2b except for (a) monthly mean cloud droplet effective radius (r_e), (b) cloud optical depth, and (c) liquid water path (LWP). ARM-retrieved properties are indicated by blue circles, and GOES-retrieved properties are shown as red asterisks. Monthly standard deviations are indicated by the error bars.

retrieved from both ARM and GOES observations. As mentioned before, July and August have less than 20 hr of samples as illustrated in Figure 1a; thus, the results in July and August should be used with caution. The yearly, seasonal, and monthly mean values of r_e, τ, and LWP are are provided in the supporting information for reference.

The monthly means for GOES and ARM r_e retrievals, differing by ~20%, yield annual means of 10.9 and 8.9 μm, respectively. GOES values are consistently higher than ARM values, with minimum and maximum differences of 1.7 μm in spring and 2.3 μm in winter, respectively. However, the standard deviations of the differences are highest in spring and summer. There do not appear to be seasonal patterns in the mean or standard deviation for either GOES or ARM, though the GOES standard deviation is lower from August to February (excepting November) and higher from March to June.

The monthly mean τ values are shown in Figure 4b with annual means of 24.5 and 26.7 for ARM and GOES, respectively. Overall, the GOES and ARM means track fairly well. ARM monthly mean τ increases from February to June, is smallest in August, and tops out in September. The GOES monthly mean τ peaks in September and generally decreases after November to summer. The ARM τ values during spring and summer are slightly greater than their GOES counterparts and a bit smaller during fall and winter. The GOES monthly standard deviations are noticeably higher for fall and winter months than during spring and summer. They also exceed the corresponding ARM monthly standard deviations for most months. The monthly mean variations of cloud LWPs from both ARM and GOES in Figure 4c are very similar to their cloud optical depths due to the small seasonal variation in the r_e averages. As expected, the largest difference in LWP occurs in winter (ARM = 120.3 versus GOES = 229.6 g/m^2), and the spring and summer differences around 10 g/m^2, with annual means of 137.0 and 187.3 g/m^2 for ARM and GOES, respectively.

Figure 5 shows the diurnal variations of r_e, τ, and LWP from both ARM and GOES. Note that the following discussion will generally disregard the results at 12 UTC and 24 UTC as these bins have very small data counts and the values shown may not be robust. As demonstrated in Figure 5a, there is no strong diurnal variation in r_e(ARM) ranging from 8.6 μm around local noon (17–19 UTC) to ~9.5 μm. Therefore, the ARM-retrieved r_e values appear to be nearly independent of solar geometry. In general, r_e(GOES) exceeds r_e(ARM) and the differences between GOES and ARM become large toward early morning and late afternoon. This pattern is evident even when neglecting 12 and 24 UTC and indicates that r_e(GOES) is highly dependent on solar geometry. The same pattern (increasing away from local noon) is seen in the standard deviations of both ARM and GOES. Overall, at times with the lowest SZAs, r_e(GOES) means and standard deviations are very close to their ARM counterparts when binned by time. The effects of solar geometry on r_e(GOES) will be further discussed later.

The hourly mean values of ARM τ and LWP are shown in Figures 5b and 5c, respectively. Their diurnal variations mimic their r_e counterparts, having little variation. The τ and LWP comparisons between ARM and GOES are similar to the r_e comparison; that is, the differences are minimal around local noon and increase toward sunrise and sunset. The GOES standard deviations are also much higher than the ARM standard deviations for most times and appear to increase from local noon to sunset. Since GOES LWP is computed based on r_e and τ, any biases found in these properties, such as with solar geometry, would propagate through to the LWP.

Scatter-density plots between ARM and GOES cloud microphysical property retrievals, as well as their PDFs and CDFs, are shown in Figure 6. Based on Figure 6a, it is clear that GOES- and ARM-retrieved r_e values are not well correlated. The shape of the density pattern is roughly circular, and the R^2 value is 0.028. The r_e(GOES) mean is ~2 μm higher than the average for ARM and has a higher standard deviation. The PDF distributions of r_e(ARM) and r_e(GOES) values basically follow normal distributions with a right skew, though the

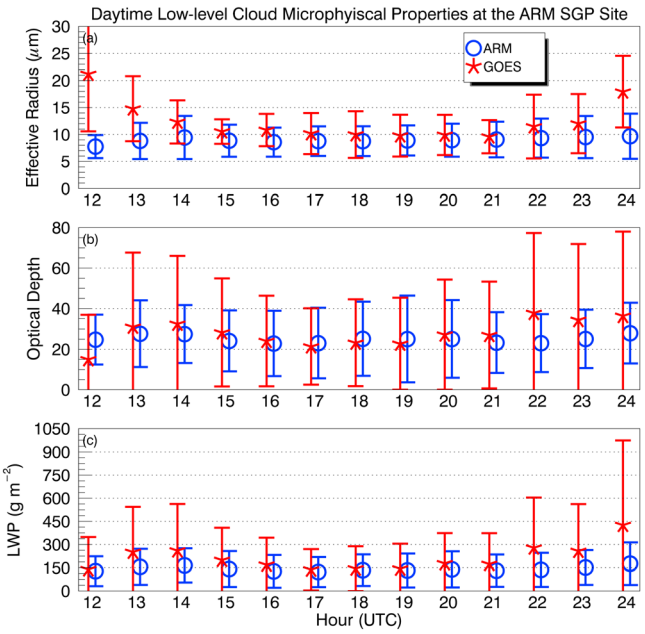

Figure 5. Same as Figure 4 except for hourly mean values.

GOES values are shifted upward by approximately 2 μm. There are two groups of outliers: the first one is for r_e(GOES) values around 12 μm while r_e(ARM) values range from 15 to 25 μm and the second one is r_e(ARM) values around 8 μm while r_e(GOES) values range from 15 to 25 μm. Points where r_e(ARM) is much higher than r_e(GOES) are distributed similarly (not shown) to the monthly and hourly distributions of the full data sample as seen in Figure 1. However, points where r_e(GOES) is much higher than r_e(ARM) preferentially occur in the morning (~66% before 15 UTC) when the solar zenith angle is high and during the spring (~50% during April and May). Also of note is that these outliers occur during the period when GOES-10 (GOES West) was used to produce these data, which will be discussed further in section 4.

Figure 6b shows the scatter-density plot for τ. In contrast to r_e, ARM- and GOES-retrieved τ values are fairly well correlated, with an R^2 of 0.45. The data density shows this as well, though the amount of scatter in the data is very high, especially for high τ values. The GOES values are on average higher than ARM with a mean difference of 2.2.Mean LWPs are 187.3 and 137.0 g/m^2 for GOES and ARM, respectively, with an R^2 of 0.47. The τ PDFs and CDFs for GOES and ARM are very similar to each other as seen in Figure 6e.

4. Sensitivities of the GOES Retrievals to Viewing and Solar Geometry

It has been mentioned that the GOES-retrieved cloud properties, especially microphysical properties, may depend on viewing and/or solar geometry. This may be a product of a seasonal sampling bias due to the SZA filter used in this study. However, this sampling bias cannot be entirely responsible for the increase in

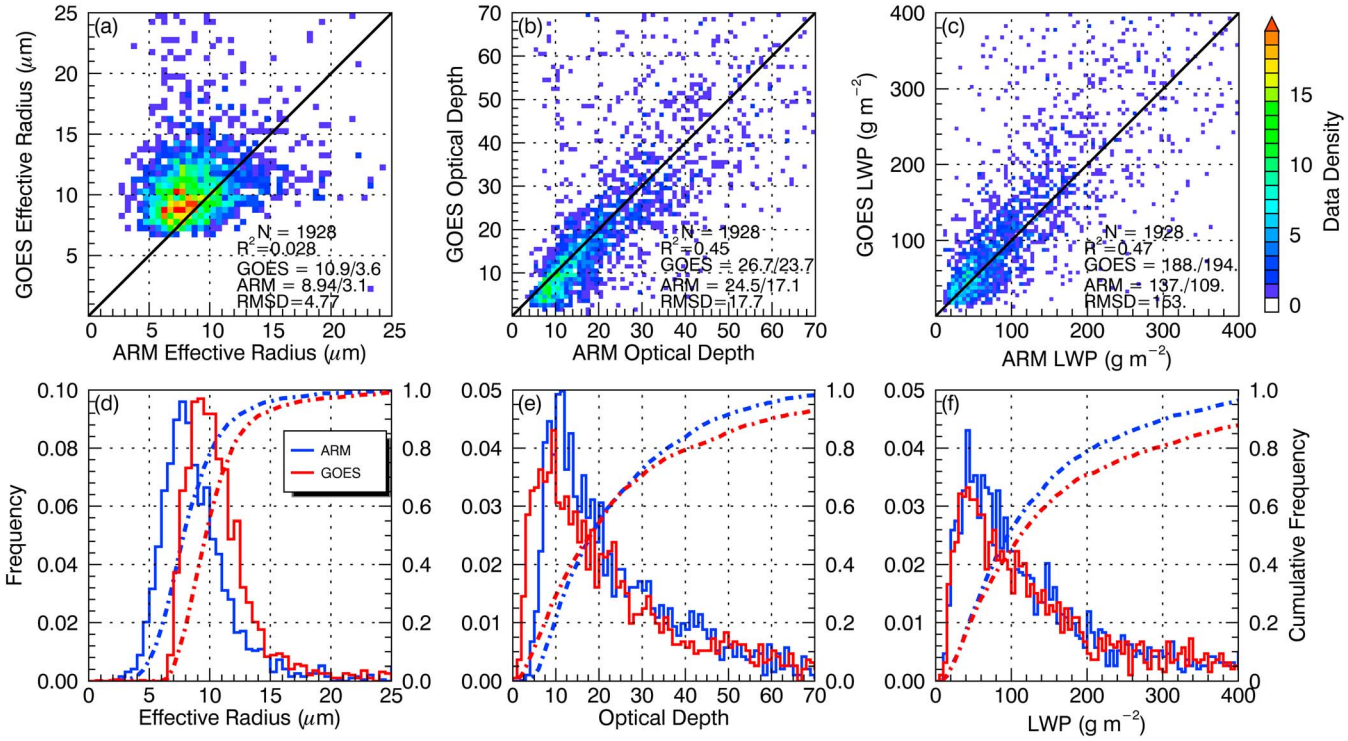

Figure 6. Same as Figure 3 except for (a and d) cloud droplet effective radius, (b and e) cloud optical depth, and (c and f) liquid water path. Note that the CDFs do not reach one for LWP or cloud optical depth because the results are highly skewed. The bin sizes are 0.5 μm, 1, and 5 g/m^2 for effective radius, optical depth, and liquid water path, respectively.

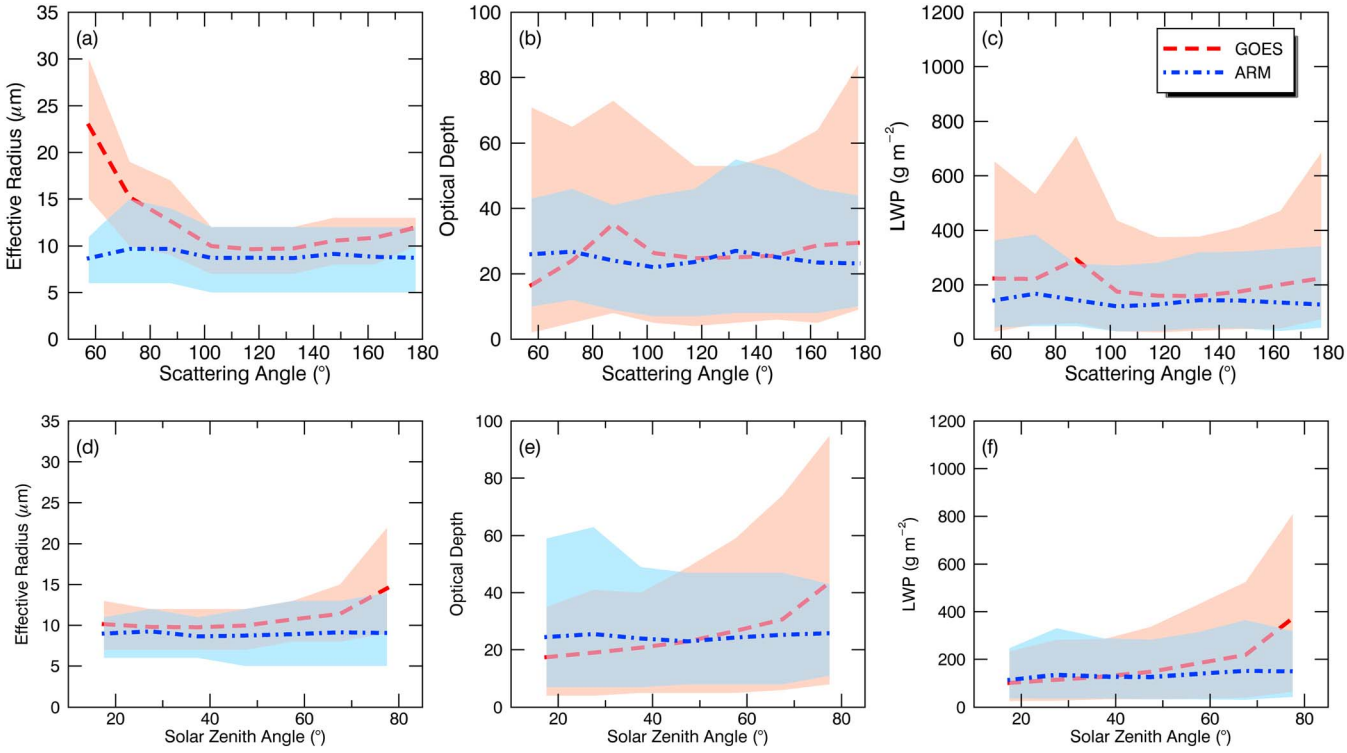

Figure 7. GOES- (red) and ARM (blue)-retrieved microphysical properties binned by (a–c) scattering angle and (d–f) solar zenith angle. Mean values for each bin are indicated by the dashed lines, and the shading shows the 10th–90th percentiles. The bin size for scattering angle is 15°, and the bin size for solar zenith angle is 10°. The numbers of data points in each bin are listed in Table 3.

GOES retrievals with increasing SZA as demonstrated in Figure 5 because the relationship is still seen from 15 UTC to 22 UTC, which are in daylight year round at the ARM SGP site. Also, because the data were produced using both GOES East and West satellites (not simultaneously), satellite viewing geometry is not constant through the data record. To examine the effects of both on GOES microphysical property retrievals, the mean and 10th–90th percentile values for bins of scattering angle (SCA, a–c) and SZA (d–f) are plotted in Figure 7. Table 3 shows the data counts by bin for reference. Here the scattering angle is defined as

$$\mathrm{SCA} = \cos^{-1}\left(-\mu\mu_0 + \mu_1\sqrt{1-\mu_0^2}\sqrt{1-\mu^2}\right),$$

where μ is the cosine of the viewing zenith angle, μ_0 is the cosine of the SZA, and μ_1 is the cosine of the relative azimuth angle. Viewing zenith angles are constant at 47° and 57° for GOES East and West, respectively. Low scattering angles indicate that the radiation scattered by cloud particles toward the satellite has a forward component (i.e., evening for GOES East and morning for GOES West).

Table 3
Bin Values and Data Counts for Figure 7

Scattering angle									
Bin (°)	$50 \le x <$ 65	$65 \le x <$ 80	$80 \le x <$ 95	$95 \le x <$ 110	$110 \le x <$ 125	$125 \le x <$ 140	$140 \le x <$ 155	$155 \le x <$ 170	$170 \le x <$ 185
Count	38	70	103	202	244	269	493	435	74
Solar zenith angle									
Bin (°)	$12.5 \le x <$ 22.5	$22.5 \le x <$ 32.5	$32.5 \le x <$ 42.5	$42.5 \le x <$ 52.5	$52.5 \le x <$ 62.5	$62.5 \le x <$ 72.5	$72.5 \le x <$ 82.5		
Count	103	188	275	325	491	308	238		

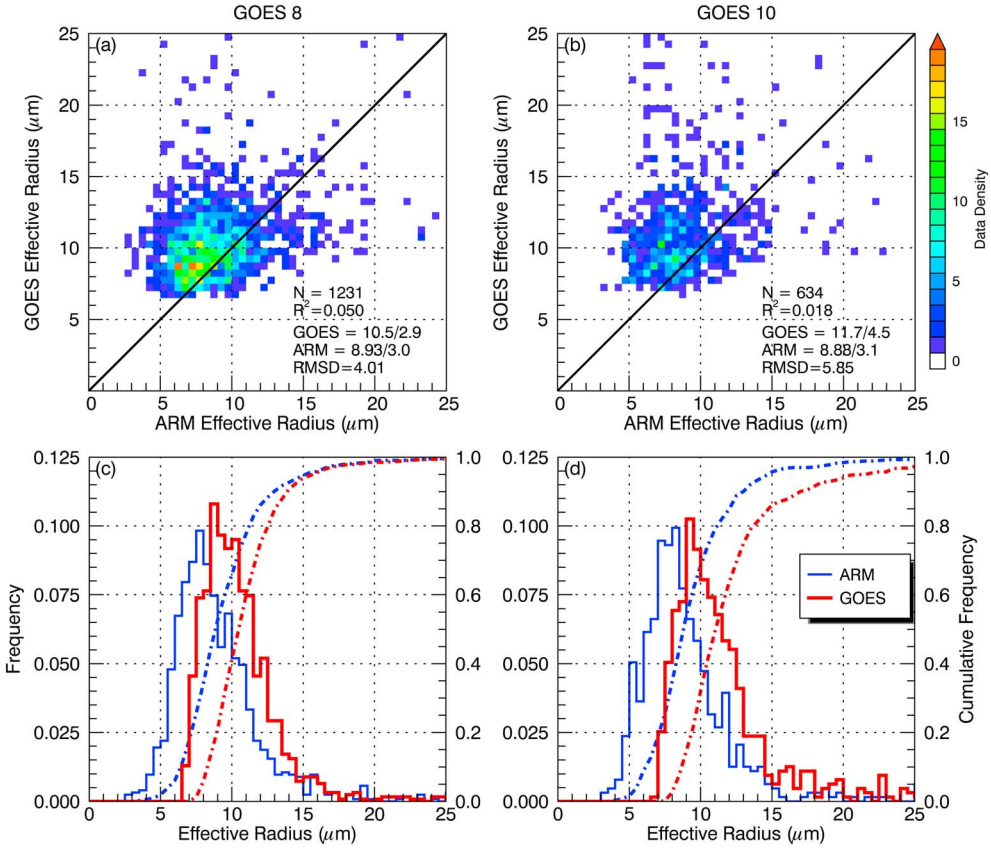

Figure 8. The same as in Figures 6a and 6d but segregated by GOES satellite. GOES 11 is not included because the data record is too short.

From the results shown in Figure 7, it is clear that the GOES-retrieved r_e, τ, and therefore LWP values all increase with increased SZA, which appears to be due higher values being retrieved almost exclusively at extreme angles. Figure 7a shows that when binned by SCA, the 10th percentile of GOES r_e is higher than the mean value from ARM under forward scattering geometry conditions. Figure 8 shows the r_e as in Figure 6, except that the data are segregated by GOES satellite. This figure suggests, based on the mean value (Figure 8b) and on the distributions (Figures 8c and 8d), that higher r_e values are more frequent for GOES 10. This makes physical sense—GOES-10 was in the GOES West position (135°W) for the data used in this study. Since it was farther away from the SGP site, the viewing geometry is more extreme, and overestimates are more likely.

Figure 9 further illustrates that the r_e bias is found only under forward scattering conditions, while muddying any conclusions that could be drawn about τ. As expected, the GOES-8 and GOES-10 mean r_e values increase and diverge greatly from ARM mean r_e when SCA is $<$90. This is especially true for GOES-10, which has lower mean SCAs. Figures 7 and 9 have demonstrated that a substantial portion of the r_e bias is due to measurements taken at SCA $<$ 90° and SZA $>$ 65°. However, the expected relationship between SCA and τ is not readily evident. The GOES-10 mean optical depths are underestimated in the morning when SCA $<$ 90°, while the GOES-8 τ means tend to be slightly overestimated at the same time, when SCA $>$ 130°, as expected. During the afternoon, the GOES-10 means are fairly close to their ARM counterparts when SCA $>$ 130°, and the GOES-8 values are overestimated when SCA $<$90°, contrary to expectations. Thus, the 3-D effects are much more complex than can be explained simply with scattering angle. Other factors, such as cloud structure orientation along a particular azimuth angle, could alter the relationship.

These problems regarding viewing/solar geometry and passive satellite cloud property retrievals stem mostly from the plane-parallel cloud assumption required for bispectral methods. These issues have been studied for a long time, with little to show for in the way of solutions. Zhang et al. (2012, 2016) discussed in detail the

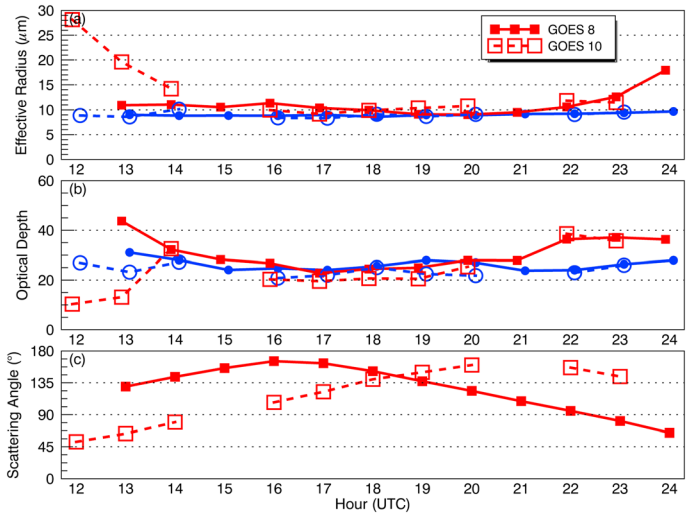

Figure 9. (a) Mean effective radius, (b) optical depth, (c) and scattering angle as a function of time and separated by satellite. GOES data are shown in red (squares), and ARM data are shown in blue (circles). Solid lines and filled symbols represent GOES-8 samples, and dashed lines and unfilled symbols represent GOES-10 retrievals.

natures of the problems and provided a comprehensive and relatively up-to-date summary of the research in this area. The biggest hurdle here is decoupling the various potential sources of error and uncertainty due to 3-D effects, subpixel level cloud inhomogeneity, and the nonlinear relationships between the reflectances and the physical parameters.

Regarding τ, Loeb and Davies (1996) showed that for stratocumulus clouds, cloud optical depths retrieved using a plane-parallel radiative transfer model increase with SZA. Loeb et al. (1998) demonstrated that this effect is primarily due to the 3-D structure of actual stratus clouds, which typically have texture of varying degrees on their tops, resulting in departures from the plane-parallel cloud assumption used for most retrieval systems. These departures include brightening in the backscattering directions and shadowing in the forward scattering directions and, therefore, respective overestimates and underestimates of retrieved τ (Horvath et al., 2014; Loeb & Coakley, 1998). This effect is clearer in Figure 7, which shows that τ is underestimated when SCA $<$ 75°. Note that this is in contrast with Varnai and Marshak (2007), which found τ to be overestimated even in the forward scattering direction. Liang and Di Girolamo (2013) attributed this discrepancy between studies to the effects of the satellite-Sun relative azimuth angle, which is likely a factor in the results here and could explain the mixed results for τ seen in Figure 9.

Vant-Hull et al. (2007) described, similar to above, how illumination and shadowing can also affect retrievals of r_e. For r_e, the brightening and shadowing result in underestimates and overestimates, respectively. This is likely reflected in the variation of r_e with SCA seen in Figure 7. Note again that the expected bias under backscattering conditions is not seen in Figure 7 or Figure 9, which could be related to the specific viewing geometry of the GOES satellites. The reflected component of the 3.9-μm radiance, the primary source for estimating r_e from GOES, is inversely proportional to r_e in a nonlinear fashion. When that radiance is greater than expected (e.g., backscatter from textured cloud), the retrieval will yield an underestimate of the effective radius, up to a point. Because the droplets absorb radiation, the reflected component is generally constant for $\tau > 8$ (Minnis et al., 1998). Thus, the reflected radiance will be unchanged by additional scattering from cloud sides and r_e will not be underestimated. Since few of the clouds observed here have $\tau < 8$ (8.3% based on ARM τ), it is not surprising that r_e shows minimal dependence on SCA when SCA $>$ 90° (Figure 7a). The opposite is true, however, for the forward scatter directions where shadowing is likely to occur. In Figure 7a, r_e rises rapidly as SCA drops from 90° to 45°. The portion of the cloud shadowed by cloud bumps increases with rising SZA and decreasing SCA. Thus, the reflected 3.9-μm radiance decreases from that expected for a plane-parallel cloud and r_e can be overestimated, even for optically thick clouds. Thus, as SZA increases, the overestimate in r_e rises in the forward scattering direction if there is any texture in the cloud top. Liang et al. (2015) showed that 3-D effects are not the only source of bias. Errors in the cloud optical depth also influence the retrieved r_e directly, if $\tau < 8$ or so, depending on the particular SCAs in the retrieval. The comparisons here are taken over only one location, so the combinations of viewing and illumination angles and, hence, the range of SCAs are limited. Different dependencies may be found over other regions having different satellite-scene angular perspectives.

The discussion here is limited to possible explanations for the observed biases in τ and r_e as relating to the satellite-solar geometry specific to this study, and there are many caveats. First, keep in mind that the biases in τ and r_e are very different for different combinations of satellite-solar geometry, such as near-nadir viewing with a small SZA. Second, the studies cited have focused on numerous different cloud regimes. For example, the theoretical discussion in Vant-Hull et al. (2007) specifically relates to broken cumulus clouds, which should have more 3-D cloud top structure than overcast stratocumulus. However, studies (e.g., Painemal et al., 2012) have shown that subpixel variation in cloud top height impacts microphysics retrievals in marine

stratocumulus clouds, though open-celled marine stratocumulus would still likely have larger biases due to 3-D effects than continental overcast stratocumulus. Third, besides the cloud top structure, subpixel level variations of the cloud properties in both the horizontal and vertical have been shown to induce significant biases (Painemal et al., 2013; Shang et al., 2015; Zhang & Platnick, 2011; Zhang et al., 2012). Because τ and r_e are correlated, it is difficult to examine them independently. Zhang et al. (2016) described a method for a quantified examination of these parameters that accounts for the relationship between them, which was put to the test in a more recent study (Werner et al., 2018).

These factors make it difficult to make a quantitative comparison between the results found in this study with those found in other studies. Vant-Hull et al. (2007) found a difference of 5 μm between shadowed and brightened clouds after removing cloud-edge pixels, but as mentioned, their focus was cumulus clouds. The present study found a mean bias of from 5 μm to over 10 μm for SCA < 90. Using model simulations with a constant SZA of 60° and simulated retrievals, Marshak et al. (2006) found biases as high as 20 μm in broken stratocumulus and attributed this bias to shadowing due to variations in cloud top height. Note that here there was no attempt to quantify the r_e bias as a function of subpixel inhomogeneity as other studies have done and the use of geostationary satellites and a single surface site limited the viewing-solar geometry. Because the methodologies, cloud regimes, and targeted microphysical properties of the studies mentioned in this section vary widely, it is difficult to directly compare to them.

5. Summary and Conclusions

The GOES-retrieved daytime single-layered low-level cloud properties have been compared with the ground-based observations and retrievals at the ARM SGP site from June 1998 to December 2006. During the 8.5-year period, a total of 964 hr of single-layered overcast clouds were selected from collocated ARM and GOES observations over the ARM SGP site. Based on the monthly and hourly means, as well as scatter-density plots of ARM and GOES cloud macrophysical and microphysical properties, the following conclusions are drawn.

1. The monthly mean GOES T_{eff} values basically follow the seasonal variations of the ARM T_{base} and T_{top} but are ~3 K colder than both T_{base} and T_{top} through the course of a year. This cold bias, which has been found in other studies, peaks in the early morning. While the diurnal variation shown here could be due to sampling bias, it fits with the hypothesis of Painemal et al. (2013) that longwave cooling and droplet evaporation may be responsible. This is still only a possible explanation, and the cloud-air temperature difference should be addressed by the cloud modeling community to ensure that stratocumulus cloud energetics are properly simulated.
2. Overall, GOES- and ARM-retrieved τ and LWP agree fairly well, while r_e is not correlated at all. The ARM-retrieved r_e, τ, and LWP values have no strong diurnal variation; therefore, the ARM microphysical properties are nearly independent of solar zenith angles (SZAs). This is not true for GOES-retrieved microphysical properties.
3. Viewing and solar geometry are important. When binned by SCA, r_e(GOES) increases with decreasing SCA, while τ is underestimated (overestimated) in forward scatter (backscatter) conditions. This is likely a result of 3-D cloud effects, such as shadowing created by variations in cloud top structure. Enhanced backscatter reflectance is more important for the τ retrieval, while shadowing (forward scatter) impacts both optical depth and effective radius at extreme SZA values. This is also confirmed by the difference in r_e(GOES) for GOES-8 and GOES-10. These conclusions on viewing and solar geometry are not unexpected and confirm what have been found in previous studies on passive remote sensing-retrieved cloud microphysical properties. Expected biases in the forward scattering direction were not found, which may be due the viewing geometry specific to the GOES satellites and the location of interest. Because the focus of this study was an overall evaluation and characterization of the GOES data, further investigation of these issues was left for future work.

GOES-retrieved terrestrial stratocumulus microphysical and macrophysical properties were evaluated against surface-based retrievals and characterizations of the uncertainties, and biases on multiple timescales are presented for users of this GOES product. This study also illustrated the known effects of viewing and illumination geometry on passive satellite microphysical property retrievals by providing long-term characterization

of biases. Subjects such as the cold bias in passively retrieved T_{eff} and the effects of viewing/solar geometry in combination with subpixel inhomogeneity should be the focus of upcoming studies, as there are major issues in remote sensing of cloud properties.

Acknowledgments
This research was supported by the NASA CERES project under grant NNX17AC52G at the University of Arizona and the NOAA R2O project with award number NA15NWS468004 at the University of North Dakota and subaward to the University of Arizona. P. Minnis and R. Palikonda are supported by the NASA CERES Project and by the DOE ARM and ASR programs under contract, DE-SC0013896. M. Thieman is supported by DOE ARM under contract, DE-SC0013896. We thank the reviewers and editors for their time. The GOES SatCORP and ARM data are available via DOE ARM Data Discovery (https://www.archive.arm.gov/discovery/).

References

Ackerman, T. P., & Stokes, G. M. (2003). The Atmospheric Radiation Measurement Program. *Physics Today*, *56*(1), 38–44. https://doi.org/10.1063/1.1554135

Ayers, J. K., Yi, Y., Minnis, P., Nguyen, L., Palikonda, R., Trepte, Q. Z., et al. (2006). Overview of NASA Langley ARM cloud products and validation. Proc. 16th ARM Sci. Team Mtg., Albuquerque, NM, March 27-31. Retrieved from https://www.arm.gov/publications/proceedings/conf16/extended_abs/ayers_jk.pdf

Benjamin, S. G., Devenyi, D., Weygandt, S. S., Brundage, K. J., Brown, J. M., Grell, G. A., et al. (2004). An hourly assimilation-forecast cycle: The RUC. *Monthly Weather Review*, *132*(2), 495–518. https://doi.org/10.1175/1520-0493(2004)132<0495:AHACTR>2.0.CO;2

Bretherton, C. S., Wood, R., George, R. C., Leon, D., Allen, G., & Zheng, X. (2010). Southeast Pacific stratocumulus clouds, precipitation and boundary layer structure sampled along 20 S during VOCALS-REx. *Atmospheric Chemistry and Physics*, *10*(21), 10,639–10,654. https://doi.org/10.5194/acp-10-10639-2010

Caldwell, P., & Bretherton, C. S. (2009). Large eddy simulation of the diurnal cycle in southeast Pacific stratocumulus. *Journal of the Atmospheric Sciences*, *66*(2), 432–449. https://doi.org/10.1175/2008JAS2785.1

Chang, F.-L., Minnis, P., Ayers, J. K., McGill, M. J., Palikonda, R., Spangenberg, D. A., et al. (2010). Evaluation of satellite-based upper troposphere cloud-top-height retrievals in multilayer cloud conditions during TC4. *Journal of Geophysical Research*, *115*, D00J05. https://doi.org/10.1029/2009JD013305

Chiu, J. C., Huang, C. H., Marshak, A., Slutsker, I., Giles, D. M., Holben, B. N., et al. (2010). Cloud optical depth retrievals from the Aerosol Robotic Network (AERONET) cloud mode observations. *Journal of Geophysical Research*, *115*, D14202. https://doi.org/10.1029/2009JD013121

Clothiaux, E. E., Ackerman, T. P., Mace, G. C., Moran, K. P., Marchand, R. T., Miller, M. A., & Martner, B. E. (2000). Objective determination of cloud heights and radar reflectivities using a combination of active remote sensors at the ARM CART sites. *Journal of Applied Meteorology*, *39*(5), 645–665. https://doi.org/10.1175/1520-0450(2000)039<0645:ODOCHA>2.0.CO;2

Clothiaux, E. E., M. Miller, R. Perez, D. Turner, K. Moran, B. Martner, T. Ackerman, et al. (2001). The ARM Millimeter Wave Cloud Radars (MMCRs) and the Active Remote Sensing of Clouds (ARSCL) Value Added Product (VAP), DOE Tech. Memo. ARM VAP-002.1, 56 pp., U. S. Dept. of energy, Washington, D. C.

Curry, J. A., Hobbs, P. V., King, M. D., Randall, D. A., Minnis, P., Isaac, G. A., et al. (2000). FIRE Arctic clouds experiment. *Bulletin of the American Meteorological Society*, *81*(1), 5–29. https://doi.org/10.1175/1520-0477(2000)081<0005:FACE>2.3.CO;2

Dong, X., Ackerman, T. P., & Clothiaux, E. E. (1998). Parameterization of microphysical and shortwave radiative properties of boundary layer stratus from ground-based measurements. *Journal of Geophysical Research*, *103*, 31,681–31,693. https://doi.org/10.1029/1998JD200047

Dong, X., Ackerman, T. P., Clothiaux, E. E., Pilewskie, P., & Han, Y. (1997). Microphysical and radiative properties of boundary layer stratiform clouds deduced from ground-based measurements. *Journal of Geophysical Research*, *102*, 23,829–23,843. https://doi.org/10.1029/97JD02119

Dong, X., & Mace, G. G. (2003). Profiles of low-level stratus cloud microphysics deduced from ground-based measurements. *Journal of Atmospheric and Oceanic Technology*, *20*, 45–53.

Dong, X., Minnis, P., Ackerman, T. P., Clothiaux, E. E., Mace, G. G., Long, C. N., & Liljegren, J. C. (2000). A 25-month database of stratus cloud properties generated from ground-based measurements at the Atmospheric Radiation Measurement Southern Great Plains Site. *Journal of Geophysical Research*, *105*(D4), 4529–4537. https://doi.org/10.1029/1999JD901159

Dong, X., Minnis, P., Mace, G. G., Smith, W. L. Jr., Poellot, M., Marchand, R. T., & Rapp, A. D. (2002). Comparison of stratus cloud properties deduced from surface, GOES, and aircraft data during the March 2000 ARM cloud IOP. *Journal of the Atmospheric Sciences*, *23*, 3265–3284.

Dong, X., Minnis, P., & Xi, B. (2005). A climatology of midlatitude continental clouds from ARM SGP site. Part I: Low-level cloud macrophysical, microphysical and radiative properties. *Journal of Climate*, *18*(9), 1391–1410. https://doi.org/10.1175/JCLI3342.1

Dong, X., Minnis, P., Xi, B., Sun-Mack, S., & Chen, Y. (2008). Comparison of CERES-MODIS stratus cloud properties with ground-based measurements at the DOE ARM Southern Great Plains site. *Journal of Geophysical Research*, *113*, D03204. https://doi.org/10.1029/2007JD008438

Dong, X., Xi, B., Kennedy, A., Minnis, P., & Wood, R. (2014). A 19-month record of marine aerosol-cloud-radiation properties derived from DOE ARM AMF deployment at the Azores: Part I: Cloud fraction and single-layered MBL cloud properties. *Journal of Climate*, *27*(10), 3665–3682. https://doi.org/10.1175/JCLI-D-13-00553.1

Dong, X., Xi, B., Qiu, S., Minnis, P., Sun-Mack, S., & Rose, F. (2016). A radiation closure study of Arctic stratus cloud microphysical properties using the collocated satellite-surface data and Fu-Liou radiative transfer model. *Journal of Geophysical Research: Atmospheres*, *121*, 10,175–10,198. https://doi.org/10.1002/2016JD025255

Dong, X., Xi, B., & Wu, P. (2014). Investigation of the diurnal variation of marine boundary layer cloud microphysical properties at the Azores. *Journal of Climate*, *27*(23), 8827–8835. https://doi.org/10.1175/JCLI-D-14-00434.1

Horvath, A., Seethala, C., & Deneke, H. (2014). View angle dependence of MODIS liquid water path retrievals in warm oceanic clouds. *Journal of Geophysical Research: Atmospheres*, *119*, 8304–8328. https://doi.org/10.1002/2013JD021355

Houghton, J. T., Ding, Y. D. J. G., Griggs, J. D., Noguer, M., van der Linden, P. J., Dai, X., et al. (2001). *Climate Change 2001: The Scientific Basis*. Cambridge: The Press Syndicate of the University of Cambridge.

Intergovernmental Panel on Climate Change (2014). Climate change 2014: Synthesis report. Contribution of working groups I, II and III to the fifth assessment report of the Intergovernmental Panel On Climate Change [Core writing team, R.K. Pachauri and L.a. Meyer (eds.)]. IPCC, Geneva, Switzerland, 151 pp.

Johnson, J. C. (1950). Measurement of the surface temperature of evaporating drops. *Journal of Applied Physics*, *21*(1), 22–23. https://doi.org/10.1063/1.699414

Kennedy, A. D., Dong, X., & Xi, B. (2013). Cloud fraction at the ARM SGP site. *Theoretical and Applied Climatology*. https://doi.org/10.1007/s00704-00013-00853-00709

Kollias, P., Tselioudis, G., & Albrecht, B. A. (2007). Cloud climatology at the Southern Great Plains and the layer structure, drizzle, and atmospheric modes of continental stratus. *Journal of Geophysical Research*, *112*, D09116. https://doi.org/10.1029/2006JD007307

Liang, L., & Di Girolamo, L. (2013). A global analysis on the view-angle dependence of plane-parallel oceanic liquid water cloud optical thickness using data synergy from MISR and MODIS. *Journal of Geophysical Research: Atmospheres*, *118*, 2389–2403. https://doi.org/10.1029/2012JD018201

Liang, L., Di Girolamo, L., & Sun, W. (2015). Bias in MODIS cloud drop effective radius for water clouds as deduced from optical thickness variability across scattering angles. *Journal of Geophysical Research: Atmospheres*, *120*, 7661–7681. https://doi.org/10.1002/2015JD023256

Liljegren, J. C., Clothiaux, E. E., Mace, G. G., Kato, S., & Dong, X. (2001). A new retrieval for cloud liquid water path using a ground-based microwave radiometer and measurements of cloud temperature. *Journal of Geophysical Research*, *106*, 14,485–14,500. https://doi.org/10.1029/2000JD900817

Loeb, N. G., & Coakley, J. A. Jr. (1998). Inference of marine stratus cloud optical depths from satellite measurements: Does 1D theory apply? *Journal of Climate*, *11*(2), 215–233. https://doi.org/10.1175/1520-0442(1998)011<0215:IOMSCO>2.0.CO;2

Loeb, N. G., & Davies, R. (1996). Observational evidence of plane parallel model biases: Apparent dependence of cloud optical depth on solar zenith angle. *Journal of Geophysical Research*, *101*, 1621–1634. https://doi.org/10.1029/95JD03298

Loeb, N. G., Varnai, T., & Winker, D. M. (1998). Influence of sub-pixel scale cloud-top structure on reflectances from overcast stratiform clouds. *Journal of the Atmospheric Sciences*, *55*(18), 2960–2973. https://doi.org/10.1175/1520-0469(1998)055<2960:IOSSCT>2.0.CO;2

Löhnert, U., & Crewell, S. (2003). Accuracy of cloud liquid water path from ground-based microwave radiometry: 1. Dependency on cloud model statistics. *Radio Science*, *38*(3), D09207. https://doi.org/10.1029/2005JD006686

Marshak, A., Platnick, S., Várnai, T., Wen, G., & Cahalan, R. F. (2006). Impact of three-dimensional radiative effects on satellite retrievals of cloud droplet sizes. *Journal of Geophysical Research*, *111*, D09207

Mather, J. H., & Voyles, J. W. (2013). The ARM climate research facility: A review of structure and capabilities. *Bulletin of the American Meteorological Society*, *94*(3), 377–392. https://doi.org/10.1175/BAMS-D-11-00218.1

McGaughey, A. J. H., & Ward, C. A. (2002). Temperature discontinuity at the surface ofan evaporating droplet. *Journal of Applied Physics*, *91*(10), 6406–6415. https://doi.org/10.1063/1.1471363

Miller, D. J., Zhang, Z., Ackerman, S. A., Platnick, S., & Baum, B. A. (2016). The impact of cloud vertical profile on liquid water path retrieval based on the bispectral method: A theoretical study based on large-eddy simulations of shallow marine boundary layer clouds. *Journal of Geophysical Research*, *121*, 4122–4141. https://doi.org/10.1002/2015JD024322

Min, Q., Duan, M., & Marchand, R. (2003). Validation of surface retrieved cloud optical properties with in situ measurements at the Atmospheric Radiation Measurement Program (ARM) south Great Plains site. *Journal of Geophysical Research*, *108*(D17), 4547. https://doi.org/10.1029/2003JD003385

Min, Q., & Harrison, L. C. (1996). Cloud properties derived from surface MFRSR measurements and comparison with GEOS results at the ARM SGP site. *Geophysical Research Letters*, *23*, 1641–1644. https://doi.org/10.1029/96GL01488

Min, Q., Minnis, P. J., & Khaiyer, M. M. (2004). Comparison of cirrus optical depths derived from GOES-8 and surface measurements. *Journal of Geophysical Research*, *109*, D15207. https://doi.org/10.1029/2003JD004390

Minnis, P., Bedka, K., Trepte, Q., Trepte, Q., Yost, C. R., Bedka, S. T., et al. (2016). A consistent long-term cloud and clear-sky radiation property dataset from the Advanced Very High Resolution Radiometer (AVHRR), Climate Algorithm Theoretical Basis Document (C-ATBD), CDRP-ATBD-0826 Rev 1 AVHRR Cloud Properties - NASA, NOAA CDR Program, 19 September, 159 pp.. https://doi.org/10.789/V5HT2M8T

Minnis, P., Garber, D. P., Young, D. F., Arduini, R. F., & Takano, Y. (1998). Parameterizations of reflectance and effective emittance for satellite remote sensing of cloud properties. *Journal of the Atmospheric Sciences*, *55*(22), 3313–3339. https://doi.org/10.1175/1520-0469(1998)055<3313:PORAEE>2.0.CO;2

Minnis, P., & Harrison, E. F. (1984). Diurnal variability of regional cloud and clear-sky radiative parameters derived from GOES data. Part II: November 1978 cloud distributions. *Journal of Climate and Applied Meteorology*, *23*(7), 1012–1031. https://doi.org/10.1175/1520-0450(1984)023<1012:DVORCA>2.0.CO;2

Minnis, P., Heck, P. W., Young, D. F., Fairall, C. W., & Snider, J. B. (1992). Stratocumulus cloud properties derived from simultaneous satellite and island-based instrumentation during FIRE. *Journal of Applied Meteorology*, *31*(4), 317–339. https://doi.org/10.1175/1520-0450(1992)031<0317:SCPDFS>2.0.CO;2

Minnis, P., Nguyen, L., Doelling, D. R., Young, D. F., Miller, W. F., & Kratz, D. P. (2002). Rapid calibration of operational and research meteorological satellite imagers. Part I: Evaluation of research satellite visible channels as references. *Journal of Atmospheric and Oceanic Technology*, *19*(9), 1233–1249. https://doi.org/10.1175/1520-0426(2002)019<1233:RCOOAR>2.0.CO;2

Minnis, P., Nguyen, L., Palikonda, R., Heck, P. W., Spangenberg, D. A., Doelling, D. R., et al. (2008). Near-real time cloud retrievals from operational and research meteorological satellites. In *Proc. SPIE Remote Sens. Clouds Atmos. XIII, Cardiff, Wales, UK, 15–18 September* (Vol. 7107–2, 8 pp.).

Minnis, P., & Smith, W. L. Jr. (1998). Cloud and radiative fields derived from GOES-8 during SUCCESS and the ARM-UAV spring 1996 flight series. *Geophysical Research Letters*, *25*, 1125–1128. https://doi.org/10.1029/98GL00301

Minnis, P., Smith, W. L., Jr. Garber, D. P., Ayers, J. K., & Doelling, D. R. (1995). Cloud properties derived from GOES-7 for the spring 1994 ARM Intensive Observing Period using version 1.0.0 of the ARM satellite data analysis program, NASA RP 1366, 59 pp.

Minnis, P., Smith, W. L. Jr., Nguyen, L., Heck, P., & Khaiyer, M. M. (2003). Near-real-time satellite cloud products for icing detection and aviation weather over the USA (no. 2003–01-2097). SAE Technical Paper.

Minnis, P., Sun-Mack, S., Young, D. F., Heck, P. W., Garber, D. P., Chen, Y., et al. (2011). CERES Edition-2 cloud property retrievals using TRMM VIRS and Terra and Aqua MODIS data, part I: Algorithms. *IEEE Transactions on Geoscience and Remote Sensing*, *49*(11), 4374–4400. https://doi.org/10.1109/TGRS.2011.2144601

Minnis, P., Trepte, Q. Z., Sun-Mack, S., Chen, Y., Doelling, D. R., Young, D. F., et al. (2008). Cloud detection in non-polar regions for CERES using TRMM VIRS and Terra and Aqua MODIS data. *IEEE Transactions on Geoscience and Remote Sensing*, *46*(11), 3857–3884. https://doi.org/10.1109/TGRS.2008.2001351

Minnis, P., Yost, C. R., Sun-Mack, S., & Chen, Y. (2008). Estimating the physical top altitude of optically thick ice clouds from thermal infrared satellite observations using CALIPSO data. *Geophysical Research Letters*, *35*, L12801. https://doi.org/10.1029/2008GL033947

Moran, K. P., Martner, B. E., Post, M. J., Kropfli, R. A., Welsh, D. C., & Widener, K. B. (1998). An unattended cloud-profiling radar for use in climate research. *Bulletin of the American Meteorological Society*, *79*(3), 443–455. https://doi.org/10.1175/1520-0477(1998)079<0443:AUCPRF>2.0.CO;2

Nguyen, L., Doelling, D. R., Minnis, P., & Ayers, J. K. (2004). Rapid technique to cross-calibrate satellite imager visible channels. *Proceedings of SPIE*, *5542*, 227–235.

Painemal, D., Minnis, P., Ayers, J. K., & O'Neill, L. (2012). GOES-10 microphysical retrievals in marine warm clouds: Multi-instrument validation and daytime cycle over the Southeast Pacific. *Journal of Geophysical Research*, *117*, D19212. https://doi.org/10.1029/2012JD017822

Painemal, D., Minnis, P., & O'Neill, L. (2013). The diurnal cycle of cloud-top height and cloud cover over the southeastern Pacific as observed by GOES-10. *Journal of the Atmospheric Sciences*, *70*(8), 2393–2408. https://doi.org/10.1175/JAS-D-12-0325.1

Painemal, D., Minnis, P., & Sun-Mack, S. (2013). The impact of horizontal heterogeneities, cloud fraction, and liquid water path on warm cloud effective radii from CERES-like Aqua MODIS retrievals. *Atmospheric Chemistry and Physics*, *13*(19), 9997–10003. https://doi.org/10.5194/acp-13-9997-2013

Painemal, D., & Zuidema, P. (2011). Assessment of MODIS cloud effective radius and optical thickness retrievals over the southeast Pacific with VOCALS-REx in situ measurements. *Journal of Geophysical Research*, *116*, D24206. https://doi.org/10.1029/2011JD016155

Randall, D. A., Khairoutdinov, M. F., Arakawa, A., & Grabowski, W. W. (2003). Breaking the cloud parameterization deadlock. *Bulletin of the American Meteorological Society*, *84*(11), 1547–1564. https://doi.org/10.1175/BAMS-84-11-1547

Rossow, W. B., & Schiffer, R. A. (1991). ISCCP cloud data products. *Bulletin of the American Meteorological Society*, *72*(1), 2–20. https://doi.org/10.1175/1520-0477(1991)072<0002:ICDP>2.0.CO;2

Saavedra, P., Battaglia, A., & Simmer, C. (2012). Partitioning of cloud water and rainwater content by ground-based observations with the Advanced Microwave Radiometer for Rain Identification (ADMIRARI) in synergy with a micro rain radar. *Journal of Geophysical Research*, *117*, D05203. https://doi.org/10.1029/2011JD016579

Sengupta, M., Clothiaux, E. E., & Ackerman, T. P. (2004). Climatology of warm boundary layer clouds at the ARM SGP site and their comparison to models. *Journal of Climate*, *17*(24), 4760–4782. https://doi.org/10.1175/JCLI-3231.1

Shang, H., Chen, L., Bréon, F. M., Letu, H., Li, S., Wang, Z., & Su, L. (2015). Impact of cloud horizontal inhomogeneity and directional sampling on the retrieval of cloud droplet size by the POLDER instrument. *Atmospheric Measurement Techniques*, *8*(11), 4931–4945. https://doi.org/10.5194/amt-8-4931-2015

Sisterson, D. L., Peppler, R. A., Cress, T. S., Lamb, P. J., & Turner, D. D. (2016). The arm Southern Great Plains (SGP) site. *Meteorological Monographs*, *57*, 6–1.

Smith, W. L., Minnis, P., Finney, H., Palikonda, R., & Khaiyer, M. M. (2008). An evaluation of operational GOES-derived single-layer cloud top heights with ARSCL over the ARM Southern Great Plains site. *Geophysical Research Letters*, *35*, L13820. https://doi.org/10.1029/2008GL034275

Stokes, G. E., Schwartz, S. E. (1994). The Atmospheric Radiation Measurement (ARM) program: Programmatic background and design of the cloud and radiation test bed, *Bulletin of the American Meteorological Society*, *75*, 1201–1221

Sun-Mack, S., Minnis, P., Chen, Y., Kato, S., Yi, Y., Gibson, S. C., et al. (2014). Regional apparent boundary layer lapse rates determined from CALIPSO and MODIS data for cloud-height determination. *Journal of Applied Meteorology and Climatology*, *53*(4), 990–1011. https://doi.org/10.1175/JAMC-D-13-081.1

Trepte, Q., Minnis, P., & Arduini, R. F. (2002). Daytime and nighttime polar cloud and snow identification using MODIS data, proc. *SPIE*, *4891*, 449–459.

Troyan, D. (2012). Merged sounding value-added product. DOE-ARM Tech. Rep., DOE/SC-ARM/TR-087.

Vant-Hull, B., Marshak, A., Remer, L. A., & Li, Z. (2007). The effects of scattering angle and cumulus cloud geometry on satellite retrievals of cloud droplet effective radius. *IEEE Transactions on Geoscience and Remote Sensing*, *45*(4), 1039–1045. https://doi.org/10.1109/TGRS.2006.890416

Varnai, T., & Marshak, A. (2007). View angle dependence of cloud optical thicknesses retrieved by Moderate Resolution Imagsing Spectroradiometer (MODIS). *Journal of Geophysical Research*, *112*, D06203. https://doi.org/10.1029/JD2005JD006912

Werner, F., Zhang, Z., Wind, G., Miller, D. J., & Platnick, S. (2018). Quantifying the impacts of subpixel reflectance variability on cloud optical thickness and effective radius retrievals based on high-resolution ASTER observations. *Journal of Geophysical Research: Atmospheres*, *123*, 4239–4258. https://doi.org/10.1002/2017JD027916

Wielicki, B. A., Cess, R. D., King, M. D., Randall, D. A., & Harrison, E. F. (1995). Mission to planet earth: Role of clouds and radiation in climate. *Bulletin of the American Meteorological Society*, *76*(11), 2125–2153. https://doi.org/10.1175/1520-0477(1995)076<2125:MTPERO>2.0.CO;2

Wood, R. (2012). Stratocumulus clouds. *Monthly Weather Review*, *140*(8), 2373–2423. https://doi.org/10.1175/MWR-D-11-00121.1

Wood, R., Mechoso, C. R., Bretherton, C. S., Weller, R. A., Huebert, B., Straneo, F., et al. (2011). The VAMOS Ocean–Cloud–Atmosphere–Land Study Regional Experiment (VOCALS-REx): Goals, platforms, and field operations. *Atmospheric Chemistry and Physics*, *11*(2), 627–654. https://doi.org/10.5194/acp-11-627-2011

Wood, R., Wyant, M., Bretherton, C. S., Rémillard, J., Kollias, P., Fletcher, J., et al. (2015). Clouds, aerosols, and precipitation in the marine boundary layer: An arm mobile facility deployment. *Bulletin of the American Meteorological Society*, *96*(3), 419–440. https://doi.org/10.1175/BAMS-D-13-00180.1

Wu, P., Dong, X., & Xi, B. (2015). (2015). MBL drizzle properties and their impact on cloud microphysical property retrievals. *Atmospheric Measurement Techniques*, *8*(9), 3555–3562. https://doi.org/10.5194/amt-8-3555-2015

Wu, P., Dong, X., Xi, B., Liu, Y., Khaiyer, M., & Minnis, P. (2017). Effects of environment forcing on marine boundary layer cloud-drizzle processes. *Journal of Geophysical Research: Atmospheres*, *122*(8), 4463–4478. https://doi.org/10.1002/2016JD026326

Xi, B., Dong, X., Minnis, P., & Khaiyer, M. M. (2010). A 10 year climatology of cloud fraction and vertical distribution derived from both surface and GOES observations over the DOE ARM SPG site. *Journal of Geophysical Research*, *115*, D12124. https://doi.org/10.1029/2009JD012800

Xi, B., Dong, X., Minnis, P., & Sun-Mack, S. (2014). Comparison of marine boundary layer cloud properties from CERES-MODIS edition 4 and DOE ARM AMF measurements at the Azores. *Journal of Geophysical Research: Atmospheres*, *119*, 9509–9529. https://doi.org/10.1002/2014JD021813

Yan, H., Huang, J., Minnis, P., Yi, Y., Sun-Mack, S., Wang, T., & Nakajima, T. Y. (2015). Comparison of CERES-MODIS cloud microphysical properties with surface observations over Loess Plateau. *Journal of Quantitative Spectroscopy & Radiative Transfer*, *153*, 65–76. https://doi.org/10.1016/j.jqsrt.2014.09.009

Yost, C. R., Minnis, P., Ayers, J. K., Spangenberg, D. A., Heymsfield, A. J., Bansemer, A., et al. (2010). Comparison of GOES-retrieved and in situ measurements of deep convective anvil cloud microphysical properties during the Tropical Composition, Cloud and Climate Coupling Experiment (TC^4). *Journal of Geophysical Research*, *115*, D00J06. https://doi.org/10.1029/2009JD013313

Zhang, Z., Dong, X., Xi, B., Song, H., Ma, P.-L., Ghan, S. J., et al. (2017). Intercomparisons of marine boundary layer cloud properties from the ARM CAP-MBL campaign and two MODIS cloud products. *Journal of Geophysical Research: Atmospheres*, *122*, 2351–2365. https://doi.org/10.1002/2016JD025763

Zhang, Z., Ackerman, A. S., Feingold, G., Platnick, S., Pincus, R., & Xue, H. (2012). Effects of cloud horizontal inhomogeneity and drizzle on remote sensing of cloud droplet effective radius: Case studies based on large-eddy simulations. *Journal of Geophysical Research*, *117*, D19208. https://doi.org/10.1029/2012JD017655

Zhang, Z., & Platnick, S. (2011). An assessment of differences between cloud effective particle radius retrievals for marine water clouds from three MODIS spectral bands. *Journal of Geophysical Research*, *116*, D20215. https://doi.org/10.1029/2011JD016216

Zhang, Z., Werner, F., Cho, H. M., Wind, G., Platnick, S., Ackerman, A. S., et al. (2016). A framework based on 2-D Taylor expansion for quantifying the impacts of subpixel reflectance variance and covariance on cloud optical thickness and effective radius retrievals based on the bispectral method. *Journal of Geophysical Research: Atmospheres*, *121*, 7007–7025. https://doi.org/10.1002/2016JD024837